

***p*-Extension of C^0 continuous mixed finite elements for plane strain gradient elasticity**

S. MARKOLEFAS¹), T. K. PAPATHANASIOU²),
S. K. GEORGANTZINOS³)

¹) *Strength of Materials Laboratory, National and Kapodistrian University of Athens, Psachna Evias 34400, Greece*

²) *Department of Civil & Environmental Engineering, Brunel University London, UK, e-mail: theodosios.papathanasiou@brunel.ac.uk*

³) *Metallic Structures Laboratory, National and Kapodistrian University of Athens, Psachna Evias 34400, Greece*

A MIXED FINITE ELEMENT FORMULATION is developed for the general 2D plane strain, linear isotropic gradient elasticity problem. Form II of the dipolar strain gradient theory for micro-structured solids is considered. The main variables are the double stress tensor $\boldsymbol{\mu}$ and the displacement field vector \mathbf{u} . Standard C^0 -continuous, high polynomial order hierarchical basis functions are employed for the finite element solution spaces (*p*-extension). The formulation is numerically validated against the standard axial tension patch test and the Mode I crack problem. The theoretical convergence rates of the uniform *h*- and *p*-extensions are confirmed using a benchmark problem where only double stresses appear. Results for the crack problem demonstrate that proper mesh refinement at areas of steep gradients ensures reproduction of the exact solution behaviour at different length scales. More specifically, the asymptotic exponents of the crack face opening displacement and the crack head true stress solutions of the Mode I crack problem are recovered. Finally, the upper bound of the true tensile normal stress near the crack tip is estimated. This upper bound is of major importance since the nature of the exact solution may change radically as we proceed from the macro- to micro-scale.

Key words: dipolar plane strain gradient elasticity, mixed finite elements, *p*-version, mode I crack problem.

Copyright © 2019 by IPPT PAN, Warszawa

1. Introduction

AS THE DIMENSIONS OF STRUCTURES ARE SCALED DOWN to the micro- and nano-scales, e.g., in *Micro-Electro-Mechanical Systems* (MEMS) and *Nano-Electro-Mechanical Systems* (NEMS), the mechanical behaviour of materials becomes strongly size dependent [1–6]. In this case the classical elasticity theory is not able to predict phenomena like, hardening or softening behaviour [7–9], shift in resonance frequencies [10], wave dispersion [11], etc.

When the characteristic length scale of the structural component is comparable to the intrinsic length of the microstructure, strong size effects are present (e.g., in the bending of ultra-thin beams and plates, as well as, in the axial deformation of bars and membranes [3, 12–16]). Even for large scale structures, near high strain gradient areas (like corners, cracks, point loads [17], loading discontinuities [18], material properties variations [19], etc.), the strain gradient effect may be important in evaluating the local stress state, as well as, the fatigue and fracture behaviour of the material.

Analytical methods for crack problems in the framework of strain gradient elasticity can provide the asymptotic behaviour of the fields at the vicinity of the crack tip. Such results are presented e.g. in [20–22]. Closed form solutions for crack problems in a couple stress theory are also contained in [23–26]. Analytical solutions for various strain gradient elasticity problems have been obtained by several authors [17, 18, 27, 28]. However, for more complex domains and loading conditions numerical methods become a necessity. The Finite and Boundary Element methods have been employed to this end.

One of the major challenges in developing numerical methods for strain gradient elasticity problems is the order of the derivatives (typically 4th order) that appear in the differential operators present. Boundary element techniques are developed in [29, 30]. Conforming isogeometric formulations for shells and point loads for large scale structures are addressed in [31]. C^{p-1} ($p \geq 2$) and C^{p-1} ($p \geq 3$) continuous isogeometric finite elements for plane strain/stress gradient elasticity and gradient elastic Kirchhoff plates are developed in [32] and [33], respectively. It is noted that at least, C^2 -continuity is required for problems of plates [33], shells [31] and higher order gradient elasticity formulations [34], while C^1 -continuity is required for problems of gradient elastic bars and plane (strain or stress) gradient elasticity [32]. Isogeometric analysis for the Mode I crack problem in focus is developed in [35].

Four node quadrilateral elements, based on the Hermite type shape functions are introduced in [36]. Higher order C^1 -continuous elements are employed in [37, 38]. Mixed finite element methods can be used to suppress the increased regularity needed in the finite element interpolation schemes. Various mixed formulations for gradient elasticity or couple stress theory problems have been developed [39–44]. Other finite element methods, which aim at bypassing the C^1 -continuity requirements, may be found in [45–47].

Two dimensional strain gradient elasticity solutions, based on linear and non-linear constitutive relations are given in [48]. A general construction process of second-order isotropic moduli for 2D strain gradient elasticity is developed in [49]. A procedure for the identification of the constitutive parameters of a strain gradient elasticity model, along with criteria to assess its validity range are given in [50]. The apparent elastic properties of nano-objects, based on second strain

gradient elasticity theory are evaluated in [51]. Lagrangian Mechanics based variational formulations of higher order strain gradient elasticity theories are presented in [52].

In this study, a mixed finite element is proposed for the general 2D plane strain, linear isotropic gradient elasticity problem (Form II dipolar strain gradient theory for micro-structured solids [53]). It is noted that in the dipolar strain gradient theory, the strain energy density assumes the form of a positive-definite function of the strain tensor (as in classical elasticity) and the gradient of the strain tensor [7, 21, 48, 54–56]. As a result of that (in addition to the standard monopolar tractions and stresses), dipolar tractions are introduced in the formulation, resulting in dipolar (or double) stresses [53, 57, 58]. The theory is a useful limiting case of the more general theory developed in [53].

The main variables of the mixed formulation are the double stress tensor ($\boldsymbol{\mu}$) and the displacement field vector (\boldsymbol{u}). The current μ - u formulation is embedded in the general category of mixed methods developed in [59] (see also [40, 60, 61]). High order, C^0 -continuous, conforming basis functions are employed in the form of the p -version or p -extension [62, 63]. The resulting weak forms, as well as the stiffness matrices of the discrete approximations, exhibit the standard (symmetric) mixed structure [64–66].

The advantage of the current mixed formulation is that it avoids the requirement of C^1 -continuity where both the values and the derivatives of the main variables must be continuous across inter-element boundaries. In addition to that, the true stress function, which includes third order derivatives of the displacement field, can be computed (post-processed) based on the first order derivatives of the main variables $\boldsymbol{\mu}$ and \boldsymbol{u} . Finally, all the non-standard boundary conditions (including the jump conditions at the corners [55, 57, 59]) are embedded formally and straightforwardly, either in the weak formulation or in the solution spaces as essential conditions. This study extends previous results for anti-plane shear [40] gradient elasticity problems to the plane strain case. In this setting several problems (see for examples in [1–4, 21]) can be effectively treated with the proposed finite element scheme. To the best of the authors' knowledge, this is the first p -extension based mixed finite element formulation for plane strain gradient elasticity. In addition, the present study verifies the theoretically predicted convergence and asymptotic rates through applications in computationally demanding problems (e.g. crack opening).

The paper is organized as follows: the governing equations of the 2D plane strain gradient elasticity problem are summarized in Section 2. The current mixed finite element formulation is developed in Section 3. Numerical experimentations are presented in Section 4, including Mode I crack stress analysis (in plane strain conditions). The final section, Section 5, contains closing remarks, conclusions and future research directions.

2. Governing equations for 2D plane strain isotropic dipolar gradient elasticity

Henceforth, isotropic material behaviour and plane strain conditions (in the plane x, y or 1, 2) are assumed. The simple gradient elasticity model, with one characteristic length constant associated with the microstructure is considered [14, 21, 54].

Standard tensorial (or indicial) notation is employed in the current work (the summation convention is employed for repeated indices). Let u_i denote the displacement components, τ_{ij} the Cauchy stress, ε_{ij} the standard strain, μ_{ijk} the double stress and κ_{ijk} the strain gradient components ($i, j = 1$ or 2). Recall furthermore that $\varepsilon_{ij} := \frac{1}{2}(u_{i,j} + u_{j,i})$, $\kappa_{ijk} := \varepsilon_{jk,i}$ (Form II) and $(*)_{,i} := \frac{\partial(*)}{\partial x_i} = \partial_i(*)$.

Regarding the standard plane strain problem ($\varepsilon_{33} = \varepsilon_{13} = \varepsilon_{23} = 0$, $\partial_3(*) = 0$), the following relations can be derived (for details, see [7, 21, 36]).

Standard in plane strain – Cauchy stress relations:

$$(2.1) \quad \begin{Bmatrix} \varepsilon_{11} \\ \varepsilon_{22} \\ \varepsilon_{12} \end{Bmatrix} = \begin{bmatrix} C_{11} & C_{12} & 0 \\ C_{12} & C_{22} & 0 \\ 0 & 0 & C_{33} \end{bmatrix} \begin{Bmatrix} \tau_{11} \\ \tau_{22} \\ \tau_{12} \end{Bmatrix} \quad \text{or} \quad \varepsilon_{ik} = C_{ij}\tau_{jk}, \quad i, j = 1, 2$$

where

$$(2.2) \quad C_{11} = C_{22} = \frac{(1+\nu)(1-\nu)}{E}, \quad C_{12} = -\frac{\nu(1+\nu)}{E}, \quad C_{33} = \frac{(1+\nu)}{E}$$

and E, ν are the Young's modulus and Poisson's ratio, respectively.

Double stress – Cauchy stress relations:

$$(2.3) \quad \mu_{ijk} = g^2 \tau_{jk,i}, \quad i, j, k = 1, 2$$

where $g > 0$ is a (small) constant (with units of length), the so-called *gradient coefficient*, which is associated with intrinsic material length(s) [20, 26] and (or) to microarchitecture [67].

The strain gradient – double stress relations follow from Eqs. (2.1), (2.3), using the definition of the strain gradient,

$$(2.4) \quad \kappa_{ijk} = \varepsilon_{jk,i} = C_{jm}\tau_{mk,i} = g^{-2}C_{jm}\mu_{imk}.$$

The Form II formulation has been employed in the development of the above equations (recall the symmetry $\mu_{ijk} = \mu_{ikj}$). The equilibrium equations of the gradient elasticity theory are as follows [21, 53, 57, 59],

$$(2.5) \quad \partial_j(\tau_{jk} - \partial_i\mu_{ijk}) + f_k = 0,$$

where f_k denotes the body forces.

Using (2.4) and (2.5), as well as, the definitions of strain and strain gradient, a coupled system of two fourth-order partial differential equations is derived for the two components, u_1, u_2 of the displacement field. However, the development of the current mixed formulation is based on Eqs. (2.4) and (2.5).

The above equations are accompanied with suitable boundary conditions. The structure of the boundary conditions, which depend on the particular application, may be deduced by proper reduction from the general gradient elasticity boundary conditions [21, 55, 57]. Assuming that the surface double traction, as well as, the body double force are absent, the general theory boundary conditions are stated as follows,

- *traction boundary conditions:*

$$(2.6a) \quad n_j(\tau_{jk} - \partial_i \mu_{ijk}) - D_j(n_i \mu_{ijk}) + (D_l n_l) n_j n_i \mu_{ijk} = t_k \quad \text{on } S_{N,t}^k.$$

- *moment boundary conditions:*

$$(2.6b) \quad n_i n_j \mu_{ijk} = 0 \quad \text{on } S_{N,m}^k.$$

- *jump conditions:*

$$(2.6c) \quad [m_j n_i \mu_{ijk}] = 0 \quad \text{on } C$$

where:

n_j – components of the outward unit vector normal to the surface,

τ_{ij} – components of the (symmetric) *Cauchy* stress tensor,

μ_{ijk} – components of the double stress tensor,

t_k – components of the surface (true) traction (force per unit area),

$D_j(*) := (\delta_{jl} - n_j n_l) \partial_l (*)$ – surface gradient operator.

δ_{jl} – components of the *Kronecker* delta operator,

C – boundary manifold(s), where the normal unit vectors exhibit jumps (i.e., corner points in 2D domain, surface edges in 3D domain),

$[y]$ – the difference of the values of quantity y between both sides of the corner point(s) or edge(s) C ,

$m_j := e_{lkj} s_l n_k$, where s_l denotes the components of the tangential vector of curve C and e_{lkj} is the (well-known) *alternating tensor*.

Regarding the domain, $S_{N,t}^k$ denotes the part of the boundary where the k component of the right hand side of the traction condition Eq. (2.6a) is specified (a given point of the boundary either belongs to $S_{N,t}^k$ or the displacement field u_k must be specified on this point, i.e., $S_{N,t}^k \cup S_{E,t}^k = S$, $S_{N,t}^k \cap S_{E,t}^k = \emptyset$). $S_{N,m}^k$ is the part of the boundary where the k component of the right hand side of the moment condition (2.6b) is specified (a given point of the boundary either belongs to $S_{N,m}^k$ or the normal derivative $Du_k := n_l \partial_l u_k$ must be specified on this point, i.e., $S_{N,m}^k \cup S_{E,m}^k = S$, $S_{N,m}^k \cap S_{E,m}^k = \emptyset$). It is noted that $S := \partial\Omega$,

$S_{E,t}^k$ denotes the boundary part where u_k is prescribed and $S_{E,m}^k$ denotes the part where Du_k is specified.

In order to fully clarify the above nomenclature, a two dimensional domain with straight line boundary curves, parallel to x or y axis (see Fig. 2) is considered. Using Eq. (2.6), several boundary condition cases that can be formulated (the intermediate algebra is omitted and all indices span the values 1 and 2) are included in Table 1.

Table 1. Boundary conditions for the plane strain gradient elasticity model.

Boundary Condition Type	Boundary Condition Expression
Boundary curve (parallel to the y axis) which is part of $S_{N,t}^k$ with applied true traction t_k	$n_1(\tau_{1k} - \partial_1\mu_{11k} - \partial_2\mu_{21k} - \partial_2\mu_{12k}) = t_k$
Boundary curve (parallel to the x axis) which is part of $S_{N,t}^k$ with applied true traction t_k	$n_2(\tau_{2k} - \partial_1\mu_{12k} - \partial_2\mu_{22k} - \partial_1\mu_{21k}) = t_k$
Boundary curve (parallel to the y axis) which is part of $S_{N,m}^k$	$\mu_{11k} = 0$
Boundary curve (parallel to the x axis) which is part of $S_{N,m}^k$	$\mu_{22k} = 0$
Boundary curve (parallel to the x or y axis) which is part of $S_{E,t}^k$	$u_k = 0$
Boundary curve (parallel to the y axis) which is part of $S_{E,m}^k$	$\frac{\partial u_k}{\partial x} = u_{k,1} = 0$
Boundary curve (parallel to the x axis) which is part of $S_{E,m}^k$	$\frac{\partial u_k}{\partial y} = u_{k,2} = 0$
Jump conditions at the (right angle) corners, see (2.6 c), $s_1 = s_2 = 0$, $s_3 = +1$	$\mu_{121} + \mu_{211} = 0, \quad \mu_{122} + \mu_{212} = 0$
Anti-symmetry conditions	<ul style="list-style-type: none"> • If a parallel to x axis boundary line is an axis of anti-symmetry: $\mu_{221} = 0, \quad u_1 = 0, \quad u_{2,2} = 0$ • If a parallel to y axis boundary line is an axis of anti-symmetry, then $\mu_{112} = 0, \quad u_2 = 0, \quad u_{1,1} = 0$
Symmetry conditions	<ul style="list-style-type: none"> • If a parallel to x axis boundary line is an axis of symmetry: $\mu_{211} = \mu_{222} = 0, \quad u_2 = 0, \quad u_{1,2} = 0$ • If a parallel to y axis boundary line is an axis of symmetry: $\mu_{111} = \mu_{122} = 0, \quad u_1 = 0, \quad u_{2,1} = 0$

For plane strain conditions, the non-zero double stress components are depicted in Fig. 1. The out-of-plane components, $\mu_{i33} = g^2\tau_{33,i}$, $i, j = 1, 2$ do not enter the formulation. These components may be post-computed, based on the derivatives of the normal (out-of-plane) Cauchy stress τ_{33} . The latter depends only on the in-plane Cauchy stress components, τ_{11} and τ_{22} (through the Hooke's law).

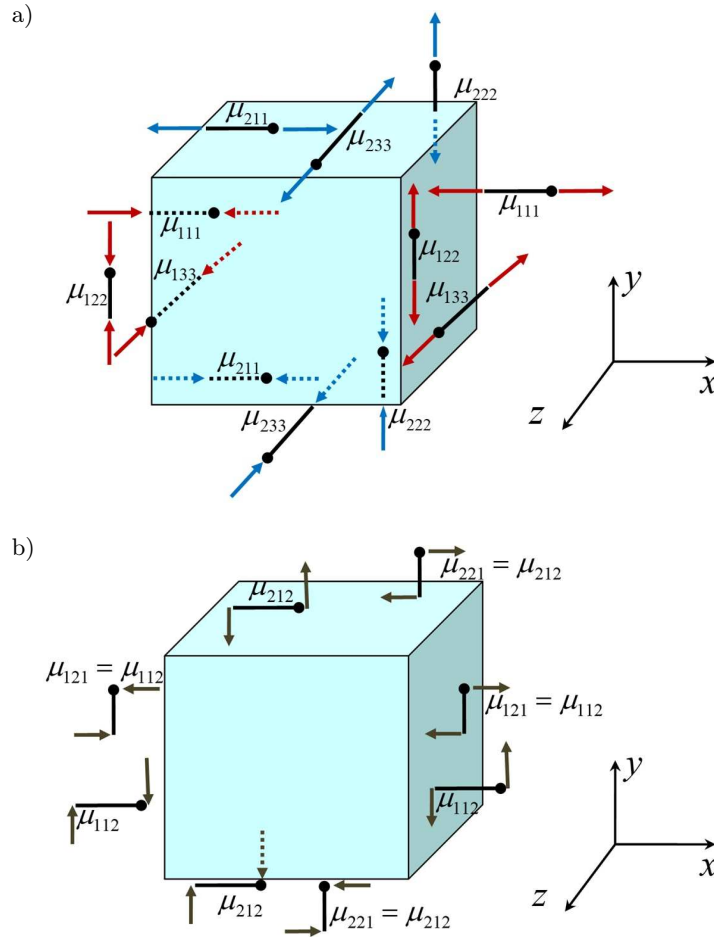


FIG. 1. Plane Strain conditions in xy plane – Non vanishing Double Stress Components – 2D strain gradient elasticity (FORM II) – Double Stress components of the form (a) $\mu_{\alpha k k}$, $\alpha = 1, 2, k = 1, 2, 3$, 12 components total, and (b) $\mu_{\alpha\beta\gamma}$, $\alpha, \beta, \gamma = 1, 2, \beta \neq \gamma$, 8 components total (components on both positive and negative faces are shown).

3. Development of the mixed finite element formulation

Let r_{ijk} be proper weighting functions associated with the double stress components μ_{ijk} . In all the following relations the indices take the values 1 and 2. Then from (2.4) there follows,

$$(3.1) \quad \int_{\partial\Omega} n_i r_{ijk} \frac{1}{2} (u_{j,k} + u_{k,j}) dS - \int_{\Omega} r_{ijk,i} \frac{1}{2} (u_{j,k} + u_{k,j}) d\Omega = \int_{\Omega} \frac{C_{jm}}{g^2} r_{ijk} \mu_{imk} d\Omega.$$

Using the symmetry $r_{ijk} = r_{ikj}$ we finally get,

$$(3.2) \quad \int_{\Omega} \frac{C_{jm}}{g^2} r_{ijk} \mu_{imk} d\Omega + \int_{\Omega} r_{ijk,i} u_{j,k} d\Omega = \int_{\partial\Omega} n_i r_{ijk} u_{j,k} dS.$$

The standard decomposition is employed on the right hand side

$$(3.3) \quad \partial_j u_k = D_j u_k + n_j D u_k$$

to get

$$(3.4) \quad \int_{\Omega} \frac{C_{jm}}{g^2} r_{ijk} \mu_{imk} d\Omega + \int_{\Omega} r_{ijk,i} u_{j,k} d\Omega - \int_{\partial\Omega} n_i r_{ijk} (D_j u_k) dS = \int_{\partial\Omega} n_i r_{ijk} n_j D u_k dS,$$

where $D u_k := n_l \partial_l u_k$ is the normal derivative of u_k .

Note that the double stress condition $n_i n_j \mu_{ijk} = 0$, see Eq. (2.6b) is essential for the current mixed formulation, whereas the conjugate condition $D u_k = 0$ is natural. Moreover, the tangential derivatives of the displacement field on the boundary contribute to the stiffness matrix (through the line integral).

Next, we multiply the equilibrium equation (2.5) by a proper weight function s_k , associated with the displacement field and integrate over the problem domain.

$$(3.5) \quad \int_{\Omega} s_k \partial_j (\tau_{jk} - \partial_i \mu_{ijk}) d\Omega + \int_{\Omega} s_k f_k d\Omega = 0.$$

Application of the Gauss theorem and the traction boundary condition Eq. (2.6a) results in the following equation,

$$(3.6) \quad \int_{\Omega} \mu_{ijk,i} s_{k,j} d\Omega + \int_{\partial\Omega} D_j (n_i \mu_{ijk}) s_k dS - \int_{\partial\Omega} (D_l n_l) n_j n_i \mu_{ijk} s_k dS - \int_{\partial\Omega} \tau_{jk} s_{k,j} d\Omega = - \int_{\Omega} s_k f_k d\Omega - \int_{\partial\Omega} t_k s_k dS.$$

Using the identity,

$$(3.7) \quad \int_{\partial\Omega} D_j (n_i \mu_{ijk}) s_k dS = \int_{\partial\Omega} D_j (n_i \mu_{ijk} s_k) dS - \int_{\partial\Omega} D_j (s_k) n_i \mu_{ijk} dS,$$

as well as, the surface divergence theorem, it follows,

$$(3.8) \quad \int_{\partial\Omega} D_j(n_i\mu_{ijk})s_k dS = \int_{\partial\Omega} (D_l n_l)n_j n_i \mu_{ijk} s_k dS + \oint_C [m_j n_i \mu_{ijk}] s_k dc - \int_{\partial\Omega} D_j(s_k)n_i \mu_{ijk} dS.$$

Substituting (3.8) into (3.6) and assuming zero jump conditions, see Eq. (2.6c), we get

$$(3.9) \quad \int_{\Omega} \mu_{ijk,i} s_{k,j} d\Omega - \int_{\partial\Omega} D_j(s_k)n_i \mu_{ijk} dS - \int_{\Omega} \tau_{jk} s_{k,j} d\Omega = - \int_{\Omega} s_k f_k d\Omega - \int_{\partial\Omega} t_k s_k dS.$$

Finally, we use the Cauchy stress-strain relation to get

$$(3.10) \quad \int_{\Omega} \mu_{ijk,i} s_{k,j} d\Omega - \int_{\partial\Omega} D_j(s_k)n_i \mu_{ijk} dS - \int_{\Omega} C_{jm}^{-1} \frac{1}{2} (u_{m,k} + u_{k,m}) s_{k,j} d\Omega = - \int_{\Omega} s_k f_k d\Omega - \int_{\partial\Omega} t_k s_k dS.$$

Using the standard nomenclature for Sobolev spaces [65, 66], Eqs. (3.4) and (3.10) may be expressed in the following standard mixed formulation structure [59, 64, 65],

Exact weak mixed formulation:

Find $\mu := (\mu_{111}, \mu_{112}, \mu_{122}, \mu_{211}, \mu_{212}, \mu_{222}) \in U$ and $u := (u_1, u_2) \in Q$ such that

$$(3.11a) \quad A(\mu, r) + B(r, u) = F(r), \quad \forall r \in U,$$

$$(3.11b) \quad B(\mu, s) - C(u, s) = G(s), \quad \forall s \in Q,$$

where $r := (r_{111}, r_{112}, r_{122}, r_{211}, r_{212}, r_{222}) \in U$, $s := (s_1, s_2) \in Q$, $U \subset H^1(\Omega)^6$, $Q \subset H^1(\Omega)^2$ and

$$(3.12a) \quad A(\mu, r) := \int_{\Omega} \frac{C_{jm}}{g^2} r_{ijk} \mu_{imk} d\Omega,$$

$$(3.12b) \quad B(r, u) := \int_{\Omega} r_{ijk,i} u_{j,k} d\Omega - \int_{\partial\Omega} n_i r_{ijk} (D_j u_k) dS,$$

$$(3.12c) \quad C(u, s) := \int_{\Omega} C_{jm}^{-1} \frac{1}{2} (u_{m,k} + u_{k,m}) s_{k,j} d\Omega,$$

$$(3.12d) \quad F(r) := \int_{\partial\Omega} n_i r_{ijk} n_j D u_k dS,$$

$$(3.12e) \quad G(s) := - \int_{\Omega} s_k f_k d\Omega - \int_{\partial\Omega} t_k s_k dS.$$

The exact structure of subspaces U and Q depends on the specific boundary conditions. More specifically, we have $n_i n_j \mu_{ijk} = n_i n_j r_{ijk} = 0$ on $S_{N,m}^k$ and $u_k = 0$ on $S_{E,t}^k$. Both conditions are essential for the current formulation. Mixed type conditions relating displacements and double forces, Robin type conditions, as well as, inclined support conditions can be easily introduced in the given mixed formulation.

Note that the bilinear form $A(\mu, r)$ is coercive (hence, positive definite) on the space $L^2(\Omega)^6$ and the bilinear form $C(u, s)$ is coercive on Q (assuming non-zero essential conditions for the displacement field, i.e., no rigid body motions). Mathematical analysis regarding solution uniqueness and stability of the above general mixed formulation may be found in [59].

The discretization of the above exact weak form proceeds as follows. Let $U^p \subset U$ and $Q^p \subset Q$ be finite dimensional subspaces. The subspaces U^p and Q^p are built with globally C^0 -continuous, hierarchical, piecewise polynomial basis functions, defined on straight side quadrilateral (finite) elements, using bilinear coordinate mapping (p -extension [62]). The hierarchical elemental shape functions are based on (integrals of) the Legendre polynomials, see [63] for details. The finite element formulation is stated as follows,

Find $\mu^p := (\mu_{111}^p, \mu_{112}^p, \mu_{122}^p, \mu_{211}^p, \mu_{212}^p, \mu_{222}^p) \in U^p$ and $u^p := (u_1^p, u_2^p) \in Q^p$ such that

$$(3.13a) \quad A(\mu^p, r^p) + B(r^p, u^p) = F(r^p), \quad \forall r^p \in U^p,$$

$$(3.13b) \quad B(\mu^p, s^p) - C(u^p, s^p) = G(s^p), \quad \forall s^p \in Q^p,$$

where $r^p := (r_{111}^p, r_{112}^p, r_{122}^p, r_{211}^p, r_{212}^p, r_{222}^p) \in U^p$, $s^p := (s_1^p, s_2^p) \in Q^p$.

Finite element interpolations of equal polynomial orders are used for all main variables of the current mixed formulation. Let $N_{1j}, N_{2j}, N_{3j}, N_{4j}, N_{5j}, N_{6j}$ and N_{7j}, N_{8j} be the global basis (or local shape) functions associated with the double stress $\mu_{111}^p, \mu_{112}^p, \mu_{122}^p, \mu_{211}^p, \mu_{212}^p, \mu_{222}^p$ and the displacement field components, u_1^p, u_2^p , respectively. Then, for the typical main variable ρ_k ($k = 1, \dots, 8$) we have,

$$(3.14) \quad \rho_k = \sum_{j=1}^M d_j N_{kj},$$

Table 2. Typical stiffness matrix block of the mixed finite element method.

	$\mu_{111} (N_{1j})$	$\mu_{112} (N_{2j})$	$\mu_{122} (N_{3j})$	$\mu_{211} (N_{4j})$	$\mu_{212} (N_{5j})$	$\mu_{222} (N_{6j})$	$u_1 (N_{7j})$	$u_2 (N_{8j})$
$r_{111} N_{1i}$	$\int_{\Omega} C_{11} \frac{N_{1i} N_{1j}}{g^2} d\Omega$	0	$\int_{\Omega} C_{12} \frac{N_{1i} N_{3j}}{g^2} d\Omega$	0	0	0	$\int_{\Omega} N_{1i,1} N_{7j,1} d\Omega$	0
$r_{112} N_{2i}$	0	$\int_{\Omega} 2C_{33} \frac{N_{2i} N_{2j}}{g^2} d\Omega$	0	0	0	0	$\int_{\Omega} N_{2i,1} N_{7j,2} d\Omega$ $-\int_S N_{2i} N_{7j,2} n_1 dS$	$\int_{\Omega} N_{2i,1} N_{8j,1} d\Omega$
$r_{122} N_{3i}$	$\int_{\Omega} C_{12} \frac{N_{3i} N_{1j}}{g^2} d\Omega$	0	$\int_{\Omega} C_{22} \frac{N_{3i} N_{3j}}{g^2} d\Omega$	0	0	0	0	$\int_{\Omega} N_{3i,1} N_{8j,2} d\Omega$ $-\int_S N_{3i} N_{8j,2} n_1 dS$
$r_{211} N_{4i}$	0	0	0	$\int_{\Omega} C_{11} \frac{N_{4i} N_{4j}}{g^2} d\Omega$	0	$\int_{\Omega} C_{12} \frac{N_{4i} N_{6j}}{g^2} d\Omega$	$\int_{\Omega} N_{4i,2} N_{7j,1} d\Omega$ $-\int_S N_{4i} N_{7j,1} n_2 dS$	0
$r_{212} N_{5i}$	0	0	0	0	$\int_{\Omega} 2C_{33} \frac{N_{5i} N_{5j}}{g^2} d\Omega$	0	$\int_{\Omega} N_{5i,2} N_{7j,2} d\Omega$	$\int_{\Omega} N_{5i,2} N_{8j,1} d\Omega$ $-\int_S N_{5i} N_{8j,1} n_2 dS$
$r_{222} N_{6i}$	0	0	0	$\int_{\Omega} C_{12} \frac{N_{6i} N_{4j}}{g^2} d\Omega$	0	$\int_{\Omega} C_{22} \frac{N_{6i} N_{6j}}{g^2} d\Omega$	0	$\int_{\Omega} N_{6i,2} N_{8j,2} d\Omega$
$s_1 N_{7i}$	$\int_{\Omega} N_{7i,1} N_{1j,1} d\Omega$	$\int_{\Omega} N_{7i,2} N_{2j,1} d\Omega$ $-\int_S N_{7i,2} N_{2j} n_1 dS$	0	$\int_{\Omega} N_{7i,1} N_{4j,2} d\Omega$ $-\int_S N_{7i,1} N_{4j} n_2 dS$	$\int_{\Omega} N_{7i,2} N_{5j,2} d\Omega$	0	$-\int_{\Omega} E_{11} N_{7i,1} N_{7j,1} d\Omega$ $-\int_{\Omega} \frac{E_{33}}{2} N_{7i,2} N_{7j,2} d\Omega$	$-\int_{\Omega} E_{12} N_{7i,1} N_{8j,2} d\Omega$ $-\int_{\Omega} \frac{E_{33}}{2} N_{7i,2} N_{8j,1} d\Omega$
$s_2 N_{8i}$	0	$\int_{\Omega} N_{8i,1} N_{2j,1} d\Omega$	$\int_{\Omega} N_{8i,2} N_{3j,1} d\Omega$ $-\int_S N_{8i,2} N_{3j} n_1 dS$	0	$\int_{\Omega} N_{8i,1} N_{5j,2} d\Omega$ $-\int_S N_{8i,1} N_{5j} n_2 dS$	$\int_{\Omega} N_{8i,2} N_{6j,2} d\Omega$	$-\int_{\Omega} E_{12} N_{8i,2} N_{7j,1} d\Omega$ $-\int_{\Omega} \frac{E_{33}}{2} N_{8i,1} N_{7j,2} d\Omega$	$-\int_{\Omega} E_{22} N_{8i,2} N_{8j,2} d\Omega$ $-\int_{\Omega} \frac{E_{33}}{2} N_{8i,1} N_{8j,1} d\Omega$

where M is the total number of degrees of freedom (d.o.f.) per variable, at the global level (or at the elemental level, if we refer to the elemental shape functions) and d_j are unknown parameters to be evaluated (note that $d_j = d_j(k)$ depends on $k = 1, \dots, 8$).

Table 3. Typical force vector block of the mixed finite element method.

$r_{111}(N_{1i})$	$\int_S N_{1i} \frac{\partial u_1}{\partial x_1} n_1 dS$
$r_{112}(N_{2i})$	$\int_S N_{2i} \frac{\partial u_2}{\partial x_1} n_1 dS$
$r_{122}(N_{3i})$	0
$r_{211}(N_{4i})$	0
$r_{212}(N_{5i})$	$\int_S N_{5i} \frac{\partial u_1}{\partial x_2} n_2 dS$
$r_{222}(N_{6i})$	$\int_S N_{6i} \frac{\partial u_2}{\partial x_2} n_2 dS$
$s_1(N_{7i})$	$-\int_{\Omega} N_{7i} f_1 d\Omega - \int_S N_{7i} t_1 dS$
$s_2(N_{8i})$	$-\int_{\Omega} N_{8i} f_2 d\Omega - \int_S N_{8i} t_2 dS$

The structure of the typical block of the (global or elemental) stiffness matrix of the above mixed finite element formulation, for the case of boundary lines parallel to x and y axis, is depicted in great detail in Table 2. The respective typical global (or elemental) force vector block is shown in Table 3. The generalization for curved boundaries is straightforward (only the structure of the boundary line integrals is affected).

When we refer to the local (elemental) level, the values i, j of indices ranging from 1 to 4, correspond to the standard bilinear shape functions (of polynomial order $p = 1$). The values i, j of indices greater than 4 are associated with the higher order hierarchical shape functions (or higher order corrections), of polynomial order $p \geq 2$ (i.e., the side modes and internal or bubble modes for $p \geq 4$ and certain values of i, j greater than 16). For more details, on the construction of the hierarchical shape functions and the standard numbering at the elemental level, see [63].

4. Numerical results

Three different model problems are considered. The first model example (simple axial tension of a rectangular domain) exhibits linear displacement field and serves as a consistency test (or patch test). This example verifies that the proposed mixed finite element formulation captures the linear exact solution for arbitrary geometry quadrilateral elements, as well as, for arbitrarily varying element sizes.

The second example is used to verify the standard rates of convergence of the uniform h - and p - extensions. The forcing functionals and the boundary conditions of the general mixed form (3.11) are set up so that the exact solution includes only the double stress $\mu_{222} = \sin(x) \sin(y)$, defined on the square domain $\Omega := (0, 2\pi)^2 \subset \mathbb{R}^2$.

The third example refers to the Mode I crack problem in the framework of isotropic dipolar plain strain gradient elasticity. The exact solution for the true stress field is highly singular near the crack tip, varying as $O(r^{-3/2})$ within a neighborhood of $O(g)$, $c = g^2$ [21]. The last model problem verifies the ability of the current mixed formulation to capture the exact solution behaviour at different length scales, provided that proper mesh refinement has been performed.

4.1. Model Problem 1 (Patch Test): linear displacement field (pure Cauchy axial stress state)

The problem geometry and boundary conditions are shown in Fig. 2a. The exact solution fields are given by,

$$(4.1) \quad u_1 = -\nu \frac{P}{E} y, \quad u_2 = \frac{P}{E} y, \quad \mu_{ijk} = 0,$$

where

$$t_2 = P \left[\frac{\text{Force}}{\text{Length}^2} \right]$$

is the externally applied true traction along y axis.

Based on extensive numerical experimentation, for any rectangular domain of area $L \times B$, arbitrary material properties and general quadrilateral meshes of arbitrary polynomial order, the finite element solution coincides with the exact solution. Moreover, using the finite element mesh of Fig. 3 and the data of Fig. 2b for any polynomial order p , the axial tension exact solution $t_2 = P = 10$ is captured at all scales (mesh refinement levels).

4.2. Model Problem 2: benchmark problem with non-zero double stresses

The purpose of the current example is to test the standard rates of convergence of the uniform h - and p -extensions. This provides an indication for the quasi-optimality of the formulation. The forcing functionals of the mixed weak form (3.11) are computed so that the exact solution of the problem is $\mu_{222} = \sin(x) \sin(y)$ on the square domain $\Omega := (0, 2\pi)^2 \subset \mathbb{R}^2$. The material properties are the same as in model problem 1.

Figure 4a gives the h -extension convergence of the relative error in the H^1 semi-norm, with respect to the inverse of the non-dimensional element size parameter (in a log-log scale). More specifically, $1/h = 2$ means 2×2 elements

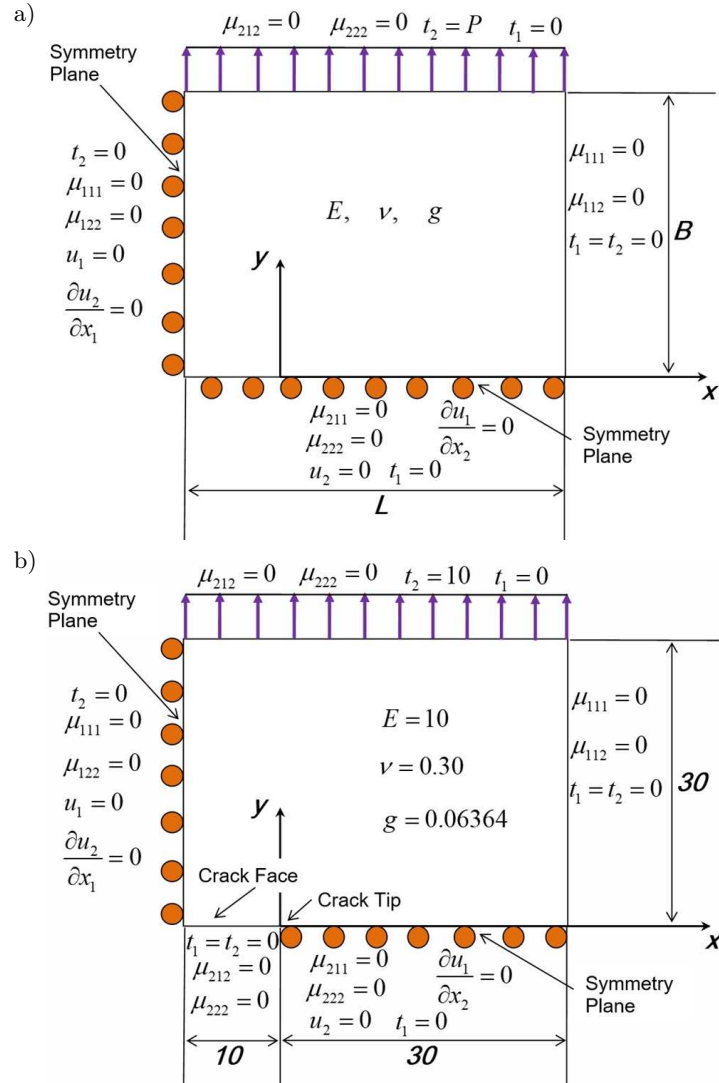


FIG. 2. Upper right quarter of (a) a slab subjected to axial tension along y axis, and (b) a cracked slab subjected to axial tension along y axis (Mode I). Problem geometry and Boundary Conditions, based on symmetry and Plane Strain Gradient Elasticity Theory.

uniform mesh, $1/h = 4$ means 4×4 elements uniform mesh etc. The relative error is defined as

$$(4.2) \quad E_{r1} := 100 \frac{|\mu_{222} - \mu_{222}^h|_1}{|\mu_{222}|_1},$$

where μ_{222}^h denotes the h -extension finite element solution (with constant poly-

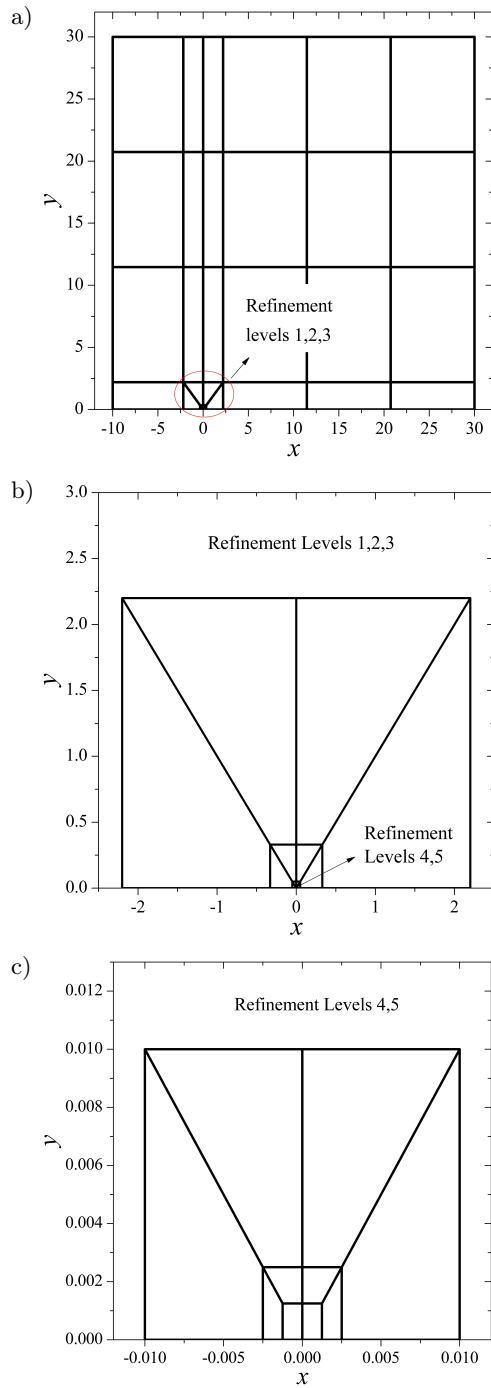


FIG. 3. Finite element mesh (a) global mesh, (b) refinement levels 1, 2, 3, and (c) refinement levels 4, 5.

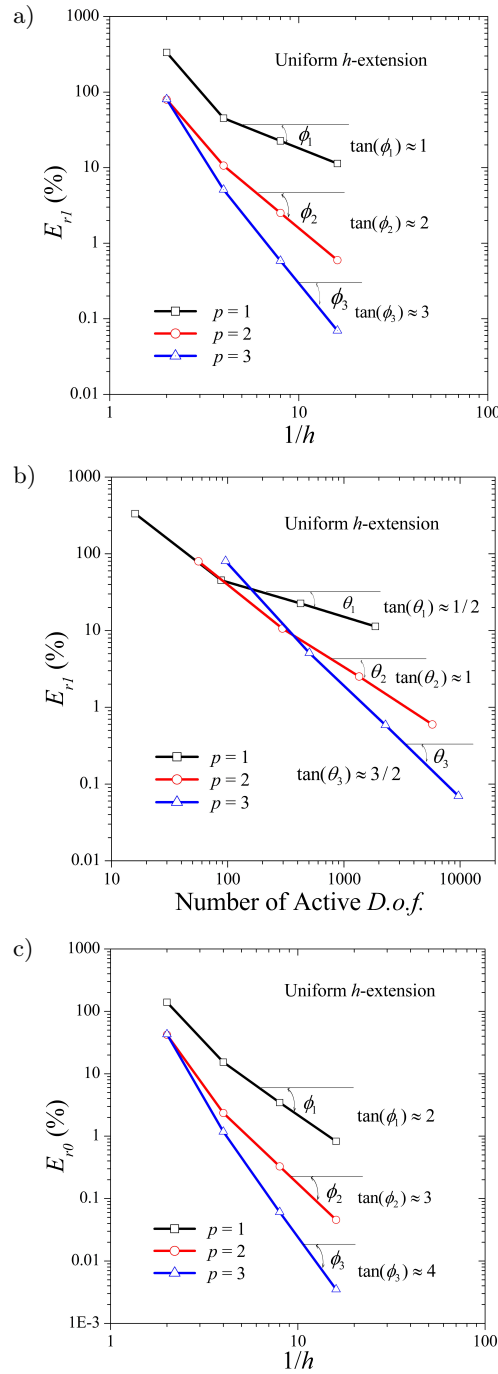


FIG. 4. Relative error in the (a) H^1 semi-norm, E_{r1} (%) vs non-dimensional element size parameter (h -extension), (b) H^1 semi-norm, E_{r1} (%) vs the number of d.o.f. (h -extension), (c) L^2 norm, E_{r0} (%) vs non-dimensional element size parameter (h -extension).

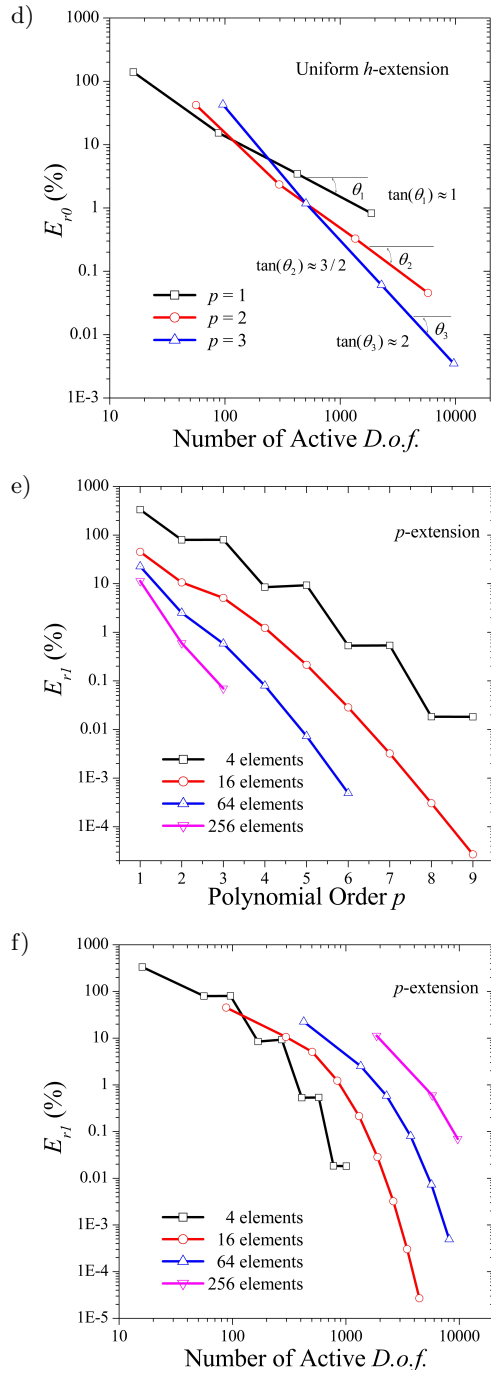


FIG. 4. [cont.] (d) L^2 norm, $E_{r,0}$ (%) vs the number of d.o.f. (h -extension), (e) H^1 semi-norm, $E_{r,1}$ (%) vs polynomial order (p -extension), (f) H^1 semi-norm, $E_{r,1}$ (%) vs the number of d.o.f. (p -extension).

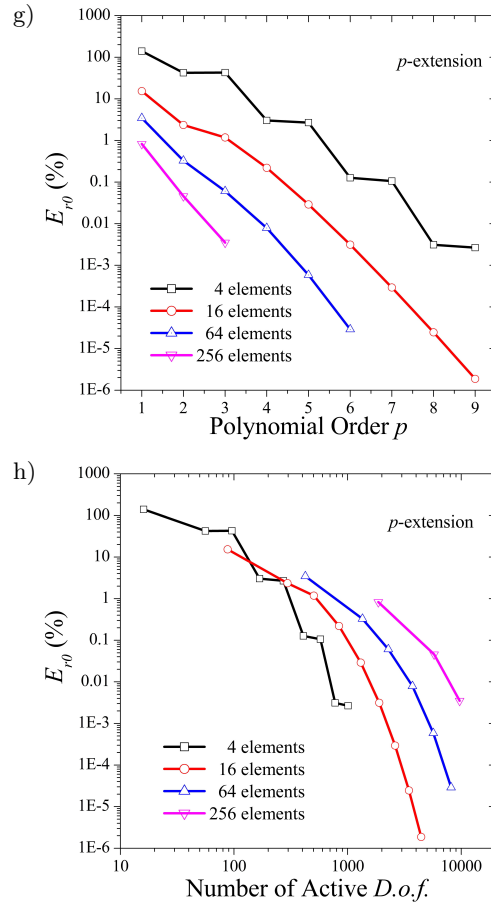


FIG. 4. [cont.] (g) L^2 norm, E_{r0} (%) vs polynomial order (p -extension), and (h) L^2 norm, E_{r0} (%) vs the number of d.o.f. (p -extension).

nomial order and increasing the number of elements uniformly) and $|y|_1 := \sqrt{\int_{\Omega} ((y_{,1})^2 + (y_{,2})^2) d\Omega}$ denotes the H^1 semi-norm of a two-dimensional scalar valued function $y(x, y)$ [62,65].

Figure 4a confirms the standard rate $E_{r1} = O(h^p)$ [62], where p is the interpolation polynomial order (for the h -extension, $p = 1, 2$ and 3 is used). Figure 4b confirms the respective rates in terms of the number of d.o.f N , $E_{r1} = O(N^{-p/2})$. Recall that asymptotically, the relation (for quasi-uniform refinement) $N \approx O(h^{-2})$ is independent of whether all or only the active d.o.f. are employed. Also, the relation $N \approx O(h^{-2})$ is independent of the number of the main variables in the formulation (the constant is different but the asymptotic behavior is the same).

Figures 4c and 4d provide the respective rates of convergence of the relative error in the L^2 norm,

$$(4.3) \quad E_{r0} := 100 \frac{\|\mu_{222} - \mu_{222}^h\|_0}{\|\mu_{222}\|_0}.$$

where $\|y\|_0 : \sqrt{\int_{\Omega} y^2 d\Omega}$ denotes the L^2 norm of a two-dimensional scalar valued function $y(x, y)$ [62, 65].

The theoretical rates $E_{r0} = O(h^{p+1})$ and $E_{r0} = O(N^{-(p+1)/2})$ are verified [62].

It is also noted that as the number of d.o.f. increases, the higher order elements are more efficient in terms of the error reduction, as compared to the lower order elements.

Figures 4e and 4f provide the p -extension convergence of the relative error in the H^1 semi-norm, with respect to the polynomial order and the number of d.o.f.

Figures 4g and 4h provide the respective p -extension convergence of the relative error in the L^2 norm. In all cases the exponential rate of convergence is confirmed [62, 63].

4.3. Model Problem 3: Mode I crack problem in 2d isotropic strain gradient elasticity

The problem geometry and boundary conditions are shown in Figure 2b. Due to symmetry considerations, the upper right quarter of the total problem domain is analyzed. The problem parameters are as follows: $c = 0.00405$ [Length²], $g = \sqrt{c} = 0.06364$ [Length], $t_2 = P = 10$ [$\frac{\text{Force}}{\text{Length}^2}$], $E = 10$ [$\frac{\text{Force}}{\text{Length}^2}$].

Based on the theoretical analysis, see [21], next to the crack tip, within a neighborhood of radius $O(g)$, the opening displacement field is $O(r^{3/2})$, where r is the distance from the crack tip. Away from this neighborhood, but still far from the external boundaries, the exact solution displacements approach the asymptotic behaviour $O(r^{1/2})$ of the standard elasticity (asymptotic) solution.

Moreover, due to gradient effects, the true stress t_2 (the y component of the true traction on a section parallel to the x axis), near the crack tip (crack head) has opposite sign from that of the elasticity solution and approaches infinity as $O(r^{-3/2})$. Far from the neighborhood of radius $O(g)$, but still near the crack tip, compared to the problem domain size, the exact true stress approaches the asymptotic behaviour $O(r^{-1/2})$ of the classical elasticity solution. Away from the crack tip, the true stress approaches the exact stress field (far field solution), derived from the standard elasticity theory for the given configuration and externally applied loads.

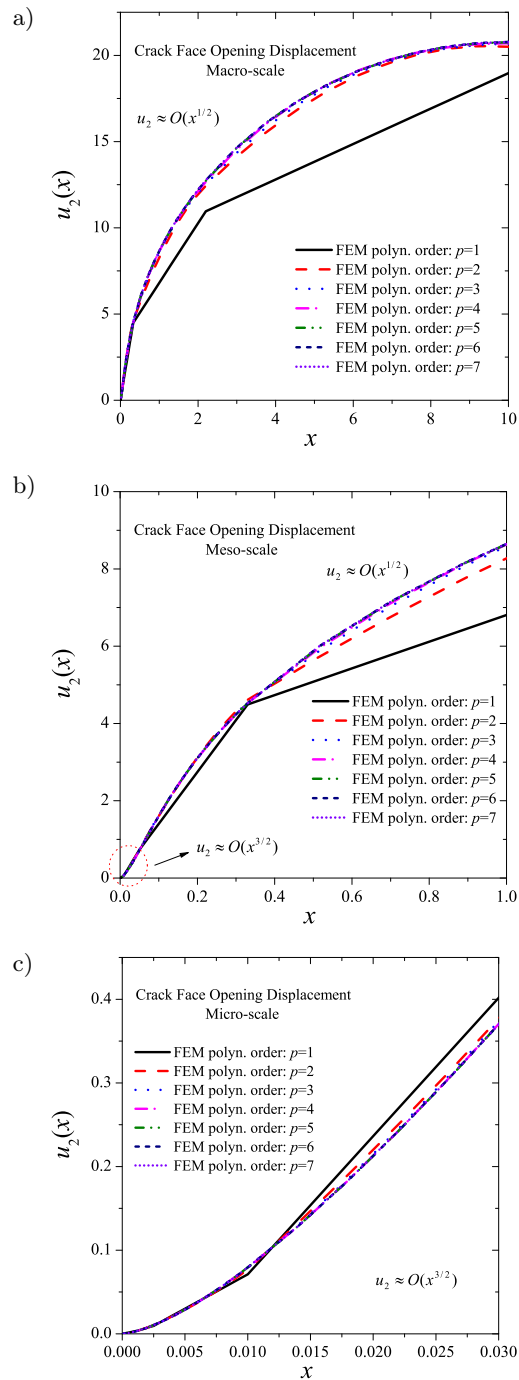


FIG. 5. Crack face opening displacement, as viewed from the (a) macro-scale, (b) meso-scale, and (c) micro-scale, for various FEM polynomial interpolation orders ($x = 0$ is at the crack tip and $0 < x < 10$ is the crack face).

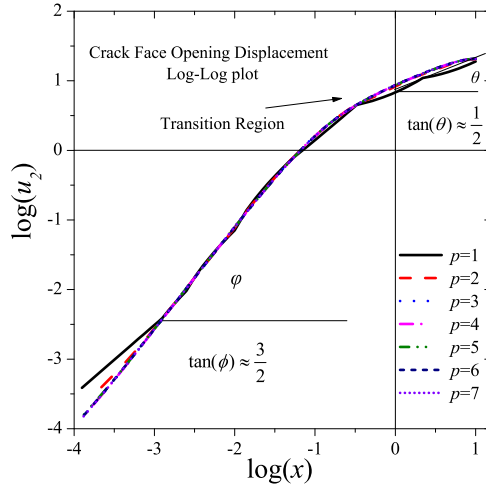


FIG. 6. Crack face opening displacement – Log-Log plot depicting the FEM Solution asymptotic exponents, at various scales of the problem.

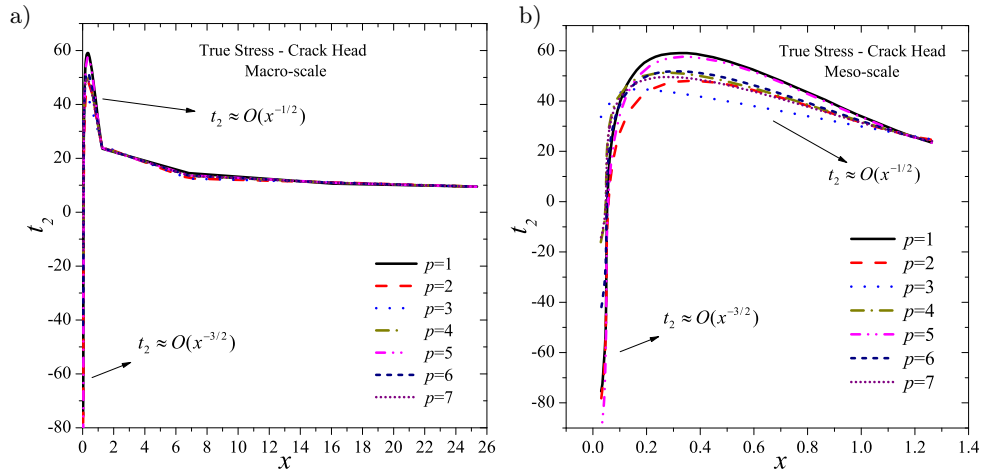


FIG. 7. Crack head true stress t_2 distribution, as viewed from the (a) macro-scale, and (b) meso-scale, for various FEM polynomial interpolation orders.

All the above are verified by the following numerical results. The mesh employed in the finite element analysis is depicted in Fig. 3. Figure 5 depicts the crack opening displacement field (crack face), at macro, meso and micro scales of the problem. By meso-scale we mean the transition region where the nature of the exact solution changes radically, from the asymptotics of the standard elasticity solution $O(r^{1/2})$ to the asymptotics of the strain gradient solution $O(r^{3/2})$,

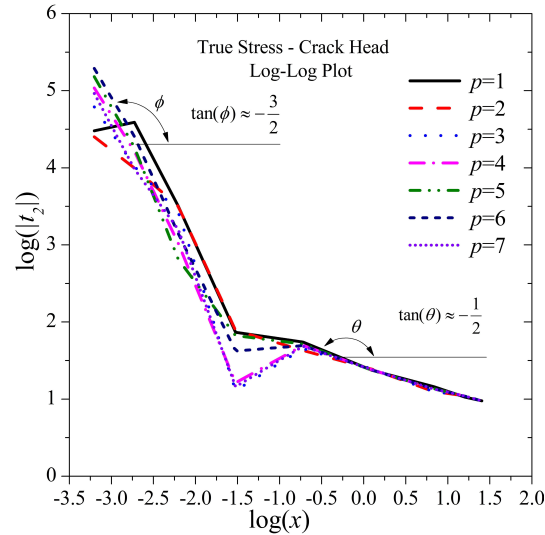


FIG. 8. Crack head true stress t_2 distribution – Log–Log plot depicting the FEM Solution asymptotic exponents at various scales of the problem (note that, for compressive stresses near the crack tip, absolute values have been used for the log-log plot).

see Fig. 6. Note that, in the vicinity of the crack tip (micro scale), the crack face opening displacement exhibits a cleaving (cusp-like) behaviour, as opposed to the classical elasticity displacement field which is more blunted.

Figure 7 depicts the distributions of the total (true) stress t_2 , ahead of the crack tip, using the finite element values at the middle of the element boundary edges. As predicted by the full field analysis [21], the true stress exhibits a local maximum at the meso-scale, see Fig. 7b. Then it reduces, reverses sign (from tensile to compressive) and becomes infinite, as $O(r^{-3/2})$, within a small neighborhood of the order $O(g)$, see Fig. 8. Our numerical experimentations reveal that the current finite element method captures the true stress local upper bound, in the vicinity of crack head, as the polynomial order increases (it is noteworthy that the convergence is not monotonic, for a fixed mesh configuration).

5. Closing discussion

A mixed formulation for the general 2D plane strain gradient elasticity problem has been developed and implemented. The current formulation employs the double stress components and the displacement field as main variables (μ - u formulation). Hierarchical, high order, C^0 -continuous, conforming basis functions were used in the finite element approximation, with equal polynomial interpolation order for all main variables. The uniform h - and p -extensions standard asymptotic convergence rates are numerically verified.

The results for the Mode I crack problem show that, with proper mesh refinement near the crack tip, the current mixed method is capable of capturing the exact solution features at various length scales. The theoretical predictions for the mode I crack problem are verified [21]. The true stress near the crack tip exhibits a local maximum positive value and the crack face opening displacement exhibits a cusp-like behaviour. The true stress upper bound is captured by the finite element solution, as the polynomial order is enhanced.

The effectiveness of the approximate solutions can be improved dramatically with proper selective polynomial refinement, based on a posteriori error estimators and adaptive techniques. Past experience can be used, as regards the development of p -adaptive degree-of-freedom error indicators (selective polynomial refinement), for similar type one dimensional mixed formulations [68]. It is noted that in [68] the error indicators are based on (local implicit residual) a posteriori error estimators, using the full local Dirichlet problems (element-by-element approximation of the mixed finite element error weak formulation).

References

1. M.H. GHAYESH, A. FARAJPOUR, *A review on the mechanics of functionally graded nanoscale and microscale structures*, International Journal of Engineering Science, **137**, 8–36, 2019.
2. A.E. GIANNAKOPOULOS, K. STAMOULIS, *Structural analysis of gradient elastic components*, International Journal of Solids and Structures, **44**, 3440–3451, 2007.
3. D.C.C. LAM, F. YANG, A.C.M. CHONG, J. WANG, P. TONG, *Experiments and theory in strain gradient elasticity*, Journal of Mechanics and Physics of Solids, **51**, 1477–1508, 2003.
4. L. LI, S. XIE, *Finite element method for linear micropolar elasticity and numerical study of some scale effects phenomena in MEMS*, International Journal of Mechanical Sciences, **46**, 1571–1587, 2004.
5. L. LU, X. GUO, J. ZHAO, *A unified size-dependent plate model based on nonlocal strain gradient theory including surface effects*, Applied Mathematical Modelling, **68**, 583–602, 2019.
6. K. STAMOULIS, A.E. GIANNAKOPOULOS, *A second gradient elasto-plastic model for fatigue of small-scale metal components*, International Journal of Structural Integrity, **1**, 3, 193–208, 2010.
7. A. CHARALAMBOPOULOS, D. POLYZOS, *Plane strain gradient elastic rectangle in tension*, Archive of Applied Mechanics, **85**, 1421–1438, 2015.
8. H. PETRYK, S. STUPKIEWICZ, *A minimal gradient-enhancement of the classical continuum theory of crystal plasticity. Part I: The hardening law*, Archives of Mechanics, **68**, 459–485, 2016.
9. S. STUPKIEWICZ, H. PETRYK, *A minimal gradient-enhancement of the classical continuum theory of crystal plasticity. Part II: Size effects*, Archives of Mechanics, **68**, 487–513, 2016.

10. D. POLYZOS, G. HUBER, G. MYLONAKIS, T. TRIANTAFYLIDIS, S. PAPARGYRI-BESKOU, D. E. BESKOS, *Torsional vibrations of a column of fine-grained material: a gradient elastic approach*, Journal of the Mechanics and Physics of Solids, **76**, 338–358, 2015.
11. S.N. ILIOPOULOS, F. MALM, C.U. GROSSE, D.G. AGGELIS, D. POLYZOS, *Concrete wave dispersion interpretation through Mindlin's strain gradient elastic theory*, Journal of the Acoustics Society of America, **142**, 1, 2017.
12. I.D. GAVARDINAS, A.E. GIANNAKOPOULOS, TH. ZISIS, *A von Karman plate analogue for solving anti-plane problems in couple stress and dipolar gradient elasticity*, International Journal of Solids and Structures, **148–149**, 169–180, 2018.
13. S. LURIE, Y. SOLYAEV, *Revisiting bending theories of elastic gradient beams*, International Journal of Engineering Science, **126**, 1–21, 2018.
14. D.M. MANIAS, T.K. PAPATHANASIOU, S.I. MARKOLEFAS, E.E. THEOTOKOGLU, *Analysis of a gradient-elastic beam on Winkler foundation and applications to nano-structure modelling*, European Journal of Mechanics A/Solids, **56**, 45–58, 2016.
15. A. TRIANTAFYLLOU, A.E. GIANNAKOPOULOS, *Structural analysis using a dipolar elastic Timoshenko beam*, European Journal of Mechanics A/Solids, **39**, 218–228, 2013.
16. G.J. TSAMASPHYROS, C.C. KOUTSOUMARIS, *Mixed nonlocal-gradient elastic materials with applications in wave propagation of beams*, International Conference of Computational Methods in Sciences and Engineering 2016 (ICCMSE 2016), AIP Conference Proceedings, 1790, 150031-1–150031-4, DOI: 10.1063/1.4968770.
17. P.A. GOURGIOTIS, TH. ZISIS, H.G. GEORGIADIS, *On concentrated surface loads and Green's functions in the Toupin–Mindlin theory of strain-gradient elasticity*, International Journal of Solids and Structures, **130–131**, 153–171, 2018.
18. H.G. GEORGIADIS, P.A. GOURGIOTIS, D.S. ANAGNOSTOU, *The Boussinesq problem in dipolar gradient elasticity*, Archives of Applied Mechanics, **84**, 1373–1391, 2014.
19. A.M. NIKOLARAKIS, E.E. THEOTOKOGLU, *Numerical analysis of transient stress field of a functionally graded nickel-zirconia profile under thermal loading*, Journal of Thermal Stresses, **38**, 10, 1085–1103, 2015.
20. H. G. GEORGIADIS, *The mode III crack problem in microstructured solids governed by dipolar gradient elasticity: static and dynamic analysis*, Journal of Applied Mechanics **70**, 517–530, 2003.
21. P.A. GOURGIOTIS, H.G. GEORGIADIS, *Plane-strain crack problems in microstructured solids governed by dipolar gradient elasticity*, Journal of the Mechanics and Physics of Solids, **57**, 1898–1920, 2009.
22. M.X. SHI, Y. HUANG, K.C. HWANG, *Fracture in a higher-order elastic continuum*, Journal of the Mechanics and Physics of Solids, **48**, 2513–2538, 2000.
23. K.P. BAXEVANAKIS, P.A. GOURGIOTIS, H.G. GEORGIADIS, *Interaction of cracks with dislocations in couple-stress elasticity. Part I: Opening mode*, International Journal of Solids and Structures, **118–119**, 179–191, 2017.
24. P.A. GOURGIOTIS, A. PICCOLROAZ, *Steady-state propagation of a Mode II crack in couple stress elasticity*, International Journal of Fracture, **188**, 119–145, 2014.
25. P.A. GOURGIOTIS, H.G. GEORGIADIS, *Distributed dislocation approach for cracks in couple stress elasticity: shear modes*, International Journal of Fracture, **147**, 83–102, 2007.

26. L. ZHANG, Y. HUANG, J.Y. CHEN, K.C. HWANG, *The mode III full-field solution in elastic materials with strain gradient effects*, International Journal of Fracture, **92**, 325–348, 1998.
27. S. KHAKALO, J. NIIRANEN, *Gradient-elastic stress analysis near cylindrical holes in a plane under bi-axial tension fields*, International Journal of Solids and Structures, **110–111**, 351–366, 2017.
28. A. KORDOLEMIS, A.E. GIANNAKOPOULOS, N. ARAVAS, *Pretwisted beam subjected to thermal loads: a gradient thermoelastic analogue*, Journal of Thermal Stresses, **40**, 10, 1231–1253, 2017.
29. G.F. KARLIS, A. CHARALAMBOPOULOS, D. POLYZOS, *An advanced boundary element method for solving 2D and 3D static problems in Mindlin’s strain-gradient theory of elasticity*, International Journal for Numerical Methods in Engineering **83**, 1407–1427, 2010.
30. G.F. KARLIS, S.V. TSINOPOULOS, D. POLYZOS, D.E. BESKOS, *Boundary element analysis of mode I and mixed mode (I and II) crack problems of 2-D gradient elasticity*, Computer Methods in Applied Mechanics and Engineering, **196**, 5092–5103, 2007.
31. V. BALOBANOV, J. KIENDL, S. KHAKALO, J. NIIRANEN, *Kirchhoff–Love shells within strain gradient elasticity: weak and strong formulations and an H^3 -conforming isogeometric implementation*, Computer Methods in Applied Mechanics and Engineering, **344**, 837–857, 2019.
32. J. NIIRANEN, S. KHAKALO, V. BALOBANOV, A.H. NIEMI, *Variational formulation and isogeometric analysis for fourth-order boundary value problems of gradient-elastic bar and plane strain/stress problems*, Computer Methods in Applied Mechanics and Engineering, **308**, 182–211, 2016.
33. J. NIIRANEN, J. KIENDL, A.H. NIEMI, A. REALI, *Isogeometric analysis for sixth-order boundary value problems of gradient-elastic Kirchhoff plates*, Computer Methods in Applied Mechanics and Engineering, **316**, 328–348, 2017.
34. S. KHAKALO, J. NIIRANEN, *Isogeometric analysis of higher-order gradient elasticity by user elements of a commercial finite element software*, Computer-Aided Design, **82**, 154–169, 2017.
35. J. NIIRANEN, S. KHAKALO, V. BALOBANOV, *Isogeometric finite element analysis of mode I cracks within strain gradient elasticity*, Journal of Structural Mechanics **50**, 337–340, 2017.
36. A. BEHESHTI, *Finite element analysis of plane strain solids in strain-gradient elasticity*, Acta Mechanica **228**, 3543–3559, 2017.
37. S. AKARAPU, H.M. ZBIB, *Numerical analysis of plane cracks in strain-gradient elastic materials*, International Journal of Fracture, **141**, 403–430, 2006.
38. P. FISCHER, J. MERGHEIM, P. STEINMANN, *On the C^1 continuous discretization of non-linear gradient elasticity: a comparison of NEM and FEM based on Bernstein–Bézier patches*, International Journal for Numerical Methods in Engineering, **82**, 1282–1307, 2010.
39. E. AMANATIDOU, N. ARAVAS, *Mixed finite element formulations of strain-gradient elasticity problems*, Computer Methods in Applied Mechanics and Engineering, **191**, 1723–1751, 2002.
40. S.I. MARKOLEFAS, D.A. TSOUVALAS, G.I. TSAMASPHYROS, *Mixed finite element formulation for the general anti-plane shear problem, including mode III crack computations, in*

- the framework of dipolar linear gradient elasticity*, Computational Mechanics, **43**, 715–730, 2009.
41. S.-A. PAPANICOLOPULOS, F. GULIB, A. MARINELLI, *A novel efficient mixed formulation for strain-gradient models*, International Journal for Numerical Methods in Engineering, **117**, 926–937, 2019.
 42. G. I. TSAMASPHYROS, S. MARKOLEFAS, D.A. TSOUVALAS, *Convergence and performance of the h - and p -extensions with mixed finite element C^0 -continuity formulations, for tension and buckling of a gradient elastic beam*, International Journal of Solids and Structures, **44**, 5056–5074, 2007.
 43. L. ZYBELL, U. MÜHLICH, M. KUNA, Z.L. ZHANG, *A three-dimensional finite element for gradient elasticity based on a mixed-type formulation*, Computational Materials Science, **52**, 1, 268–273, 2012.
 44. V. PHUNPENG, P.M. BAIZ, *Mixed finite element formulations for strain-gradient elasticity problems using the FEniCS environment*, Finite Elements in Analysis and Design, **96**, 23–40, 2015.
 45. Y. WEI, *A new finite element method for strain gradient theories and applications to fracture analyses*, European Journal of Mechanics A/Solids, **25**, 897–913, 2006.
 46. A. ZERVOS, *Finite elements for elasticity with microstructure and gradient elasticity*, International Journal for Numerical Methods in Engineering, **73**, 564–595, 2008.
 47. J. ZHAO, W. J. CHEN, S. H. LO, *A refined nonconforming quadrilateral element for couple stress/strain gradient elasticity*, International Journal for Numerical Methods in Engineering, **85**, 269–288, 2011.
 48. U. ANDREAUS, F. DELL’ISOLA, I. GIORGIO, L. PLACIDI, T. LEKSZYCKI, N.L. RIZZI, *Numerical simulations of classical problems in two-dimensional (non) linear second gradient elasticity*, International Journal of Engineering Science, **108**, 34–50, 2016.
 49. N. AUFRAY, *On the isotropic moduli of 2D strain-gradient elasticity*, Continuum Mechanics and Thermodynamics, **27**, 5–19, 2015 DOI 10.1007/s00161-013-0325-6.
 50. G. ROSI, L. PLACIDI, N. AUFRAY, *On the validity range of strain gradient elasticity: a mixed static-dynamic identification procedure*, European Journal of Mechanics/A Solids, **69**, 179–191, 2018.
 51. N.M. CORDERO, S. FOREST, E.P. BUSSO, *Second strain gradient elasticity of nano-objects*, Journal of the Mechanics and Physics of Solids, **97**, 92–124, 2016.
 52. B.E. ABALI, W.H. MÜLLER, F. DELL’ISOLA, *Theory and computation of higher gradient elasticity theories based on action principles*, Archive of Applied Mechanics, **87**, 1495–1510, 2017.
 53. R.D. MINDLIN, *Micro-structure in linear elasticity*, Archive for Rational Mechanics and Analysis, **16**, 51–78, 1964.
 54. H. ASKES, E.C. AIFANTIS, *Gradient elasticity in statics and dynamics: An overview of formulations, length scale identification procedures, finite element implementations and new results*, International Journal of Solids and Structures, **48**, 1962–1990, 2011.
 55. J.L. BLEUSTEIN, *A note on the boundary conditions of Toupin’s strain-gradient theory*, International Journal of Solids and Structures, **3**, 1053–1057, 1967.
 56. S. PAPARGYRI-BESKOU, S. TSINOPOULOS, *Lamé’s strain potential method for plane gradient elasticity problems*, Archive of Applied Mechanics, **85**, 1399–1419, 2015.

57. R.D. MINDLIN, N.N. ESHEL, *On first-gradient theories in linear elasticity*, International Journal of Solids and Structures, **4**, 109–124, 1968.
58. M. LAZAR, *Irreducible decomposition of strain gradient tensor in isotropic strain gradient elasticity*, ZAMM – Journal of Applied Mathematics and Mechanics **96**, 11, 1291–1305. 2016. DOI 10.1002/zamm.201500278.
59. S.I. MARKOLEFAS, D.A. TSOUVALAS, G.I. TSAMASPHYROS, *Theoretical analysis of a class of mixed, C^0 continuity formulations for general dipolar Gradient Elasticity boundary value problems*, International Journal of Solids and Structures, **44**, 546–572, 2007.
60. S. BALASUNDARAM, P.K. BHATTACHARYYA, *A mixed finite element method for fourth order elliptic equations with variable coefficients*, Computers and Mathematics with Applications, **10**, 245–256, 1984.
61. S. I. MARKOLEFAS, D.A. TSOUVALAS, G.I. TSAMASPHYROS, *Some C^0 -continuous mixed formulations for general dipolar linear gradient elasticity boundary value problems and the associated energy theorems*, International Journal of Solids and Structures, **45**, 3255–3281, 2008.
62. I. BABUŠKA, M. SURI, *The p - and h - p versions of the finite element method, an overview*, Computer Methods in Applied Mechanics and Engineering, **80**, 5–26, 1990.
63. B. SZABO, I. BABUŠKA, *Finite Element Analysis*, John Wiley & Sons, Inc. New York, 1991.
64. K.-J. BATHE, *The inf-sup condition and its evaluation for mixed finite element methods*, Computers and Structures, **79**, 243–252, 2001.
65. F. BREZZI, M. FORTIN, *Mixed and Hybrid Finite Element Methods*, Springer, New York, 1991.
66. F. BREZZI, K.J. BATHE, *A discourse on the stability conditions for mixed finite element formulations*, Computer Methods in Applied Mechanics and Engineering, **82**, 27–57, 1990.
67. S. KHAKALO, V. BALOBANOV, J. NIIRANEN, *Modelling size-dependent bending, buckling and vibrations of 2D triangular lattices by strain gradient elasticity models: applications to sandwich beams and auxetics*, International Journal of Engineering Science, **127**, 33–52, 2018.
68. S.I. MARKOLEFAS, D. TSOUVALAS, G. TSAMASPHYROS, *High polynomial order mixed finite element methods for strain gradient elasticity problems: a posteriori error estimation and adaptivity*, Proceedings of the 3rd International Conference “From Scientific Computing to Computational Engineering”, Athens, Greece, 9–12 July, 2008.

Received February 26, 2019; revised version June 27, 2019.

Published online August 23, 2019.
